



## LJMU Research Online

Rao, L, Liu, H, Liu, S, Shi, Z, Ren, X, Zhou, Y and Yang, Q

**Interface relationship between TiN and Ti substrate by first-principles calculation**

<http://researchonline.ljmu.ac.uk/id/eprint/9638/>

### Article

**Citation** (please note it is advisable to refer to the publisher's version if you intend to cite from this work)

**Rao, L, Liu, H, Liu, S, Shi, Z, Ren, X, Zhou, Y and Yang, Q (2018) Interface relationship between TiN and Ti substrate by first-principles calculation. Computational Materials Science, 155. pp. 36-47. ISSN 0927-0256**

LJMU has developed **LJMU Research Online** for users to access the research output of the University more effectively. Copyright © and Moral Rights for the papers on this site are retained by the individual authors and/or other copyright owners. Users may download and/or print one copy of any article(s) in LJMU Research Online to facilitate their private study or for non-commercial research. You may not engage in further distribution of the material or use it for any profit-making activities or any commercial gain.

The version presented here may differ from the published version or from the version of the record. Please see the repository URL above for details on accessing the published version and note that access may require a subscription.

For more information please contact [researchonline@ljmu.ac.uk](mailto:researchonline@ljmu.ac.uk)

# Interface relationship between TiN and Ti substrate by first-principles calculation

Lixiang Rao<sup>a</sup>, Huan Liu<sup>a</sup>, Sha Liu<sup>a</sup>, Zhijun Shi<sup>a</sup>, Xuejun Ren<sup>c</sup>, Yefei Zhou<sup>a,b</sup>, Qingxiang Yang<sup>a</sup>

<sup>a</sup> State Key Laboratory of Metastable Materials Science & Technology, Yanshan University, Qinhuangdao 066004, PR China

<sup>b</sup> College of Mechanical Engineering, Yanshan University, Qinhuangdao 066004, PR China

<sup>c</sup> School of Engineering, Liverpool John Moores University, Liverpool L3 3AF, UK

**Abstract:** In this paper, the lattice misfits between Ti and TiN interfaces were calculated by the Bramfitt two-dimensional lattice misfit theory. The adhesive work ( $W_{ad}$ ), interfacial energy ( $\gamma$ ), electronic property and bonding characteristic of  $Ti(0\ 0\ 0\ 1)/TiN(1\ 1\ 1)$  interface were also investigated by first-principles calculation. The results show that, the lattice misfit of  $Ti(0\ 0\ 0\ 1)/TiN(1\ 1\ 1)$  interface is only 2.46%, which indicates that  $Ti(0\ 0\ 0\ 1)$  and  $TiN(1\ 1\ 1)$  faces can make good lattice matching. Based on three atomic stacking modes (OT-, SL- and TL-sites) and two terminations of  $TiN(1\ 1\ 1)$  face, six kinds of  $Ti(0\ 0\ 0\ 1)/TiN(1\ 1\ 1)$  interface models were established. The interfacial bonding strength and stability of the  $Ti(0\ 0\ 0\ 1)/TiN(1\ 1\ 1)$  N-terminated (Ti/N) interface models are all larger than those of  $Ti(0\ 0\ 0\ 1)/TiN(1\ 1\ 1)$  Ti-terminated (Ti/Ti) ones.  $W_{ad}$  of the N-TL interface (Ti structure contacting with N-terminated structure of TiN with TL site) is the largest (7.97 J/m<sup>2</sup>), while the relaxed interfacial separation ( $d_0$ ) is the smallest (1.181 Å) and the  $\gamma$  is the smallest (-3.86 J/m<sup>2</sup>), which indicates that the bonding strength and stability of the N-TL interface are the largest in all interface models. Additionally, the interface bonds of Ti/Ti interface models are weak, and their interfacial strength and stability are relatively weak. The bonding strengths of the three interface models of Ti/N interfaces are larger than that of the Ti/Ti interfaces, which forms a strong polar covalent bond and a metallic one.

## 1. Introduction

Because of high specific strength, fracture toughness, corrosion resistance and thermal stability, titanium alloys have been applied for biomedical, aerospace and extreme mechanical applications and other fields [1–3]. However, because of their low hardness and wear-resistance, their application on the wear-resistance field has been restricted. Therefore, it is significant to prepare a wear resistance coating on the surface of titanium alloys. At present, surface hardening of titanium alloys includes spraying, laser and physical vapor deposition. Koshuro et al. [4] prepared the metal oxide coating on the VT6 titanium alloy by plasma spraying and micro-arc discharges, and the changes in the composition, structure and mechanical properties of the metal oxide coating were studied, which found that the microhardness of the coating is increased from  $1013 \pm 150$  HV to  $1639 \pm 31$  HV. Diao et al. [5] prepared  $TiC/TiB_2$  composite coating on TC2 titanium alloy by laser cladding method, and studied its microhardness and corrosion resistance of TC2 titanium alloy, which indicated that the hardness of the coating is three times higher than that of the TC2 alloy matrix, and the corrosion resistance of the coating is obviously higher than that of the TC2 titanium alloy matrix. Marin et al. [6] deposited CrN and TiCN coating on the surface of TC4 titanium alloy by magnetron sputtering, and took carburizing and nitriding treatment to the coating, which found that the coating after carburizing and nitriding treatment can significantly improve the tribological properties of the titanium alloy coating.

In recent years, because of its high melting point, high hardness, low friction coefficient and strong corrosion resistance, TiN has been used as a surface coating for titanium alloy workpieces widely. Kim et al. [7] investigated the effect of TiN coating on the corrosion of nano-structure  $Ti-30Ta-xZr$  alloy, which showed that the corrosion resistance of the TiN coating is higher than that of the untreated titanium alloy. Lin et al. [8] prepared TiN coating

on Ti6Al4V titanium alloy and researched the effect of TiN coating on the adhesion and corrosion resistance of bacteria, which indicated that the continuous compact coating could significantly reduce the bacterial adhesion and corrosion resistance of the Ti6Al4V substrate. Feng et al. [9] prepared the reactive plasma sprayed TiN coating and studied the friction properties of the TiN coating, which showed that the RPS-TiN coating is better than the high speed steel in the non-lubrication condition and the volume wear of the TiN coating is 2/5 of the M2 steel. However, because the TiN coating on the surface of titanium alloy workpieces is too thin, it is difficult to evaluate the binding properties by experimental method.

First-principles calculation can be used to reveal the atomic and electronic structures of interfaces, as well as the stability and cohesion of interfaces, which is widely used in material calculation [10,11]. Xiong et al. [12] calculated the interface bonding work, interfacial energy, the interface electronic structure and bonding properties of the composite coating TiB<sub>2</sub>/TiC interface by first-principles, which showed that C/Ti-terminated hollow stack (C-HS-T) exhibits the largest Wad (11.43 J/m<sup>2</sup>), the smallest interfacial separation d<sub>0</sub> (1.208 Å), which indicated that C/Ti-terminated hollow stack (C-HS-T) is the most stable. Fan et al. [13] studied the bonding and electronic properties of TiC(1 1 1)/TiN(1 1 1) interface, which indicated that the bonding properties at the interface are very similar to those of the bulk material, and the electronic transition at the interface is smooth. Liu et al. [14] calculated the electronic structure and bonding characteristic of TaN (1 1 1)/TiN(1 1 1) interface, and studied the bonding and stability of TaN(1 1 1)/TiN(1 1 1) interface as well as the bonding of atoms at the interface. However, the bonding properties between TiN coating and titanium alloy substrate by first principles calculation has not been reported before. On the basis of the Bramfitt two-dimensional lattice misfit theory, the best interface between the TiN coating and the Ti substrate for lattice matching was selected, the first principles method based on the density functional theory (DFT) was used to calculate the adhesive work, interfacial energy, electronic property and bonding characteristic of Ti(0 0 0 1)/TiN(1 1 1) interface in order to study the bonding of Ti/ TiN interface theoretically.

## 2. Calculation method

First-principles calculation based on DFT was carried out by the Vienna ab initio simulation package (VASP) [15] with the projector augmented wave (PAW) [16] method. The generalized gradient approximations (GGA) functional of Perdew-Burke-Ernzerhof (PBE) [17] were used to describe the exchange-correlation energy. For the pseudopotential, the electronic configurations are [He]2s22p3 and [Ar] 3d24s2 for nitrogen and titanium, respectively. The models used in the calculations are single unit cells of Ti bulk (1×1) and TiN bulk (1×1). In order to ensure the accuracy of the calculation, the convergence test for Kpoints and atomic wave function energy cutoff (Encut) are carried out. The Kpoints was acquired by Monkhorst-Pack method [18]. The convergence standard is that the change of the energy is less than 0.001 eV/atom between former and later energies. After a series of convergence tests (see Supplementary Figs. 1 and 2), Encut for bulk and surface calculations are set as 450 eV for Ti and 400 eV for TiN, while those for interface calculations are set as 450 eV. K points of 10×10×7, 12×12×12, 10×10×1, 12×12×1 and 12×12×1, are used for calculations for bulk Ti, bulk TiN, Ti surface, TiN surface and Ti/TiN interface, respectively. Energy change convergence value is less than 1.0×10<sup>-5</sup> eV/atom.

### 3. Results and discussion

#### 3.1. Bulk property

In order to verify the reliability of the calculation method, the GGAPBE algorithm was used to calculate the bulk properties of TiN, including lattice constants, bulk modulus (K) and formation energy (E<sub>for</sub>). The lattice constants and bulk modulus of TiN can be obtained directly from the calculated results. The E<sub>for</sub> can be obtained from the following formula Eq. (1) [19]:

$$E_{\text{for}}^{\text{TiN}} = \frac{1}{N_{\text{TiN}}} (E_{\text{TiN}}^{\text{bulk}} - E_{\text{Ti}}^{\text{bulk}} - E_{\text{N}}^{\text{bulk}}) \quad (1)$$

where  $E_{\text{for}}^{\text{TiN}}$  is the formation energy of the bulk TiN;  $E_{\text{TiN}}^{\text{bulk}}$  is the total energy of the bulk TiN;  $E_{\text{Ti}}^{\text{bulk}}$  and  $E_{\text{N}}^{\text{bulk}}$  are the energy of a Ti atom and a N atom in a single (Ti, N) system, respectively. Here the energy of the Ti atom in the  $\alpha$ -Ti and the N atom in the nitrogen molecule were employed to take the place of  $E_{\text{TiN}}^{\text{bulk}}$  and  $E_{\text{N}}^{\text{bulk}}$ , respectively.  $N_{\text{TiN}}$  is the numbers of atoms in one TiN unit cell.

The calculation results of lattice constants, K and E<sub>for</sub> of bulk TiN as well as the results of other literature [13,20–23], are listed in Table 1. From Table 1, the calculated results of TiN are in agreement with the calculated ones in other literature, and with the experimental ones, which indicates that the GGA-PBE algorithm can fully guarantee the accuracy of the calculation results.

In order to ensure the stability of the structure used in the calculation, the crystal structures of Ti and TiN are fully relaxed. The crystal structures of Ti and TiN are shown in Fig. 1. Ti structure is close-packed hexagonal one with the space group of P63/mmc (194), as shown in Fig. 1(a). The optimized primitive lattice parameters ( $a=2.923 \text{ \AA}$  and  $c=4.631 \text{ \AA}$ ) are in good agreement with other experimental values ( $a=2.951 \text{ \AA}$ ,  $c=4.686 \text{ \AA}$  [23]), which proves a good accuracy of the calculation with an error limit of 10–2  $\text{\AA}$ . From Fig. 1(b), TiN lattice structure is NaCl-type one with the space group Fm–3m (225). The lattice constant of TiN after optimization is 4.238  $\text{\AA}$ , which is basically the same as the measurement result ( $a=4.24 \text{ \AA}$ ) in Ref. [21] and the calculation result ( $a=4.33 \text{ \AA}$ ) in Ref. [13].

##### 3.1.1. Bulk property of TiN

The band structure and density of states (DOS) of bulk TiN are shown in Fig. 2. Fig. 2(a) is the band structure of TiN, in which some bands passes through the Fermi level. It indicates that TiN is of metallic character. Fig. 2(b) is the DOS of TiN. From the total DOS of TiN, two peaks at the two sides of Fermi level are located near  $-5.45 \text{ eV}$  and  $2.15 \text{ eV}$ , respectively, and the DOS between two peaks is not zero, which indicates the formation of covalent bonds. In addition, there is electron states around Fermi level, which indicates that TiN has a certain metallic character. By analysis of partial density of states (PDOS) in Fig. 2(b), it is seen that from  $-8 \text{ eV}$  to Fermi level, the peak patterns of Ti-3d electron orbital are basically the same as N-2p electron orbital, which indicates that the two orbitals overlap and form a strong covalent bond. From  $-16.7 \text{ eV}$  to  $-14.9 \text{ eV}$ , Ti-3d orbital interacts with N-2s orbital weakly, which also has a certain contribution to the covalent bonds. From the above analysis, the bonding of TiN is a mixture of metallic bond and polar covalent one. The calculation of the elastic constants for bulk TiN is helpful to study the mechanical properties of TiN. The calculated results of elastic stiffness constant ( $C_{ij}$ ) for TiN crystal structure are as follows:

$$C_{ij} = \begin{vmatrix} 657.09 & 134.03 & 134.03 & 0 & 0 & 0 \\ 134.03 & 657.09 & 134.03 & 0 & 0 & 0 \\ 134.03 & 134.03 & 657.09 & 0 & 0 & 0 \\ 0 & 0 & 0 & 161.26 & 0 & 0 \\ 0 & 0 & 0 & 0 & 161.26 & 0 \\ 0 & 0 & 0 & 0 & 0 & 161.26 \end{vmatrix}$$

TiN belongs to the cubic crystal system with only three independent elastic constants ( $C_{11}$ ,  $C_{12}$ ,  $C_{44}$ ). The elastic stiffness constant  $C_{ij}$  of TiN crystal is completely similar to the elastic compliance constant ( $S_{ij}$ ) and  $S_{ij}=C_{i-j}$ . The elastic modulus of TiN crystal structure can be estimated by two methods, namely Voigt method and Reuss method. The bulk modulus ( $K$ ) and shear modulus ( $G$ ) of TiN crystals can be obtained as follows:

$$K_V = \frac{1}{9}(C_{11} + C_{22} + C_{33}) + \frac{2}{9}(C_{12} + C_{13} + C_{23}) \quad (2)$$

$$\frac{1}{K_R} = (S_{11} + S_{22} + S_{33}) + 2(S_{12} + S_{13} + S_{23}) \quad (3)$$

$$K = \frac{1}{2}(K_V + K_R) \quad (4)$$

$$G_V = \frac{1}{15}(C_{11} + C_{22} + C_{33}) + \frac{1}{15}(C_{12} + C_{13} + C_{23}) + \frac{1}{15}(C_{44} + C_{55} + C_{66}) \quad (5)$$

$$\frac{1}{G_R} = \frac{4}{15}(S_{11} + S_{22} + S_{33}) + \frac{4}{15}(S_{12} + S_{13} + S_{23}) + \frac{4}{15}(S_{44} + S_{55} + S_{66}) \quad (6)$$

$$G = \frac{1}{2}(G_V + G_R) \quad (7)$$

where the subscript values V and R denote the Voigt and Reuss averages, respectively. K and G are the corresponding arithmetical mean values of Voigt and Reuss averages, which are called Hill approximations or Voigt-Reuss-Hill (VRH) average. Young's modulus (E) and Poisson's ratio (v) can be obtained as follows:

$$E = \frac{9KG}{3K + G} \quad (8)$$

$$v = \frac{3K-2G}{2(3K+G)} \quad (9)$$

The calculated results of the elastic properties for TiN crystal structure are listed in Table 2. The K reflects the compressive properties of the material, K of TiN crystal is  $K=308.39$  GPa, which means that TiN is not easy to be compressed. Generally,  $K/G$  is often used to reflect the toughness of the material [24]. The value of the brittle material is less than 1.75 (diamond is 0.8), and the metal material is more than 1.75 because of its better toughness. The value of TiN is 1.57, which indicates that TiN is a brittle material. The v of TiN is 0.24, which reflects its strong metallicity. The E of TiN is 485.05 GPa, and the value of austenitic stainless steel at

normal temperature is between 190 GPa and 200 GPa. It can be seen that the E of TiN is far larger than that of austenitic stainless steel, which indicates that it has strong resistance to elastic deformation.

The variations of the elastic moduli for the TiN crystal structure are listed in Table 3. In order to reflect the anisotropy of TiN more intuitively, ELATE [25] is used to analyze the spatial dependence of the elastic moduli. The spatial dependences of Young's modulus, Linear compressibility, Shear modulus and Poisson's ratio are shown in Figs. 3–6, respectively. The stronger the isotropy, the closer the three dimensional figure is to a spherical [26]. From Figs. 3–6 and Table 3, the three-dimensional graph of Linear compressibility is a very regular sphere, and the two-dimensional images of (xy), (xz) and (yz) planes are also regular circles and the anisotropy value is 1, which indicate that Linear compressibility of bulk TiN is isotropic. The three-dimensional images of the Shear modulus, Young's modulus and Poisson's ratio for bulk TiN are not spheroids, the two dimensional images of (xy), (xz) and (yz) planes also deviate from the circles, and their anisotropy values are 1.485, 1.622 and 3.1459, respectively, which indicates that the Shear modulus, Young's modulus and Poisson's ratio of bulk TiN are all with anisotropy strongly. By the above analysis, bulk TiN has strong anisotropy.

### 3.1.2. Bulk property of Ti

The calculated band structure and DOS of bulk Ti are shown in Fig. 7. From Fig. 7(a), some energy bands of Ti pass through the Fermi level, and the energy band on both sides of Fermi level fluctuates greatly. It indicates that the electronic effective mass in these energy bands is smaller and the delocalization degree is larger, which indicates that the Ti is very strong metallicity. From Fig. 7(b), by analysis of total DOS, the DOS of Ti is far greater than zero at Fermi level, which indicates that the metallicity of Ti is strong. It is consistent with the analysis result of the energy band. By analysis of PDOS, total DOS of Ti is almost all contributed by Ti-3d orbital, and the contributions of Ti-4s and Ti-3p orbitals to the DOS are very small.

## 3.2. Lattice misfit between Ti/TiN interface

When building the interface, it is necessary to determine the lattice misfit of the Ti/TiN interface. The smaller the lattice misfit, the better the lattice matching between the Ti layer and the TiN layer, and the better the interfacial adhesion and stability. The Bramfitt two-dimensional lattice misfit formula [27] is as follows:

$$\delta_{(hkl)s}^{(hkl)n} = \sum_{l=1}^3 \left[ \left( \frac{|d_{[uvw]s}^i \cos\theta - d_{[uvw]n}^i|}{d_{[uvw]n}^i} / 3 \right) \right] \times 100\% \quad (10)$$

where (h k l)s is a low-index lattice plane of nucleation substrate; (h k l)n is a low-index lattice plane of nucleation phase; [u v w]s is a low-index crystal orientation in (h k l)s; [u v w]n is a low-index crystal orientation in (h k l)n; d[uvw]s is the interatomic spacing along [u v w]s; d[uvw]n is the inter atomic spacing along [u v w]n;  $\theta$  is the angle between the [u v w]s and [u v w]n.

The calculated results are listed in Table 4. It can be seen that the lattice misfit of Ti (0 0 0 1)/TiN (1 1 1) interface is only 2.46%, which indicates that the lattice matching Ti(0 0 0 1)/TiN(1 1 1) is good. Therefore, Ti (0 0 0 1) and TiN (1 1 1) surfaces are selected to build the surface and interface models.

### 3.3. Surface convergence test

Both surface and interface models were built on periodic boundary conditions. Before the

interface model was built, the convergence tests of the Ti and TiN surface models were carried out to determine the minimum number of atomic layers when the surface model was similar to the internal structure of the bulk phase. The surface and interface models are filled with 10 Å vacuum layers to counteract interaction of the surface atom. In order to eliminate the effect of dipole, the terminations of the upper and lower surfaces of the slab are the same. The surface models of Ti and TiN are shown in Fig. 8. Fig. 8(a) is the surface model of Ti(0 0 0 1), which is a polar surface. Fig. 8(b) and (c) are TiN(1 1 1) Ti-terminated surface model and TiN(1 1 1) N-terminated surface model, respectively, which are all non-polar surfaces.

### 3.3.1. Surface energy of Ti

The convergence of surface energy with the increase of atomic number N is one of the ways to prove that the surface model achieves the phase property. Since Ti(0 0 0 1) face is a non-polar surface, the surface energy of the surface model was calculated by Botteger formula [28]:

$$\sigma_{\text{Ti}(0001)} = \frac{1}{2A} (E_{\text{slab}}^N - E_{\text{slab}}^{N-2}) \quad (11)$$

$$\Delta E = (E_{\text{slab}}^N - E_{\text{slab}}^{N-2})/2 \quad (12)$$

where  $\sigma_{\text{Ti}(0001)}$  is the surface energy of Ti(0 0 0 1) surface model;  $E_{\text{slab}}^N$  and  $E_{\text{slab}}^{N-2}$  are the total energy of surface models with N and N-2 atomic layers, respectively; A is the surface area of the surface model.

The surface energies of Ti(0 0 0 1) surface model with different atomic layers are listed in Table 5. When model atomic layers are over 6 layers, the surface energy of Ti(0 0 0 1) surface model is converged to 1.92 J/m<sup>2</sup>, which indicates that the interior of the model is similar to the bulk phase.

### 3.3.2. Surface energy of TiN

TiN(1 1 1) face is polar surface and the surface energy can be obtained by [29]:

$$\sigma_{\text{TiN}(111)} = \frac{1}{2A} (E_{\text{slab}} - N_{\text{Ti}}\mu_{\text{Ti}} - N_{\text{N}}\mu_{\text{N}}) \quad (13)$$

where  $\sigma_{\text{TiN}(111)}$  is the surface energy of TiN(1 1 1) surface model; A is the surface area of the model; E<sub>slab</sub> is the total energy of surface model; N<sub>Ti</sub> and N<sub>N</sub> are the numbers of Ti atom and N atom in surface model respectively;  $\mu_{\text{Ti}}$  and  $\mu_{\text{N}}$  are the chemical potentials of Ti atom and N atom, respectively. The TiN bulk unit energy  $\mu_{\text{TiN}}^{\text{bulk}}$  can be calculated by equation as follows:

$$\mu_{\text{Ti}} + \mu_{\text{N}} = \mu_{\text{TiN}}^{\text{bulk}} \quad (14)$$

Combining Eq. (14) with Eq. (15), the equation of  $\mu_{\text{TiN}(111)}$  with only one variable ( $\mu_{\text{N}}$ ) is as follows:

$$\sigma_{\text{TiN}(111)} = \frac{1}{2A} [E_{\text{slab}} - N_{\text{Ti}}\mu_{\text{TiN}}^{\text{bulk}} - (N_{\text{N}} - N_{\text{Ti}})\mu_{\text{N}}] \quad (15)$$

In order to simplify the calculation,  $\mu_{\text{N}}$  is regarded as  $\mu_{\text{N}}^{\text{bulk}}$  approximatively.  $\mu_{\text{N}}^{\text{bulk}}$  is the chemical potential of N atoms in TiN bulk, which are put into Eq. (15) to get  $\sigma_{\text{TiN}(111)}$  values. The surface energy of 3–11 layers TiN (1 1 1) Ti-terminated surface model is listed in Table 6.

When the number of model atomic layer is over 7 layers, the surface model of TiN (1 1 1) can converge to 4.68 J/m<sup>2</sup>, which indicates that the interior of the model is similar to the bulk phase. The surface energy of the 5–15 layers of TiN (1 1 1) N-terminated surface model is listed in Table 7. When the atomic layer number is over 11, the surface energy can converge to 2.16 J/m<sup>2</sup>, which indicates that the surface energy converges. By the above calculation, the 6 layers of Ti (0 0 0 1) surface model, the 7 layers of TiN(1 1 1) Ti-terminated surface model and the 11 layers of TiN(1 1 1) N-termination surface model are used to build the interface model and the related calculation are carried out.

### 3.4. Interfacial properties

#### 3.4.1. Interfacial structure

According to the results of above convergence, the Ti/TiN interface model is built with the 6 layers Ti(0 0 0 1) surface model and 7 layers TiN(1 1 1) Ti-terminated surface model or 11 layers TiN(1 1 1) N-terminated surface model, and the orientation relationship is Ti[2 1 1 0]/TiN[110] and Ti(0 0 0 1)/TiN(1 1 1). Three possible stacking sites, as shown in Fig. 9, are taken into account in the calculations. In Fig. 9, the OT-site represents that the interfacial Ti atom of Ti side is directly placed on the top of the surface N(Ti) atom of TiN side, SL-site represents that the interfacial Ti atom resides on the top of N(Ti) atom in the second layer of TiN slab and TL-site represents that the interfacial Ti atom locates on the top of N(Ti) atom in the third layer of TiN slab. Upper part shows a side view and lower part for top view. The interfaces of Ti and N-termination TiN are shown only. Parts of the top and bottom of interfaces have not been shown. For the convenience of expression, the interface model is simplified and named: the Ti/TiN N(Ti)-terminated interface with OT site is named N-OT(Ti-OT), the Ti/TiN N (Ti)-terminated interface with SL site is named N-SL(Ti-SL), the Ti/TiN N(Ti)-terminated interface with TL site is named as N-TL(Ti-TL).

#### 3.4.2. Adhesion work

When the interface is built, the binding strength between the interfaces can be described qualitatively by the work of adhesion ( $W_{ad}$ ), which can be defined as the reversible work required to separate an interface into two free surfaces. The larger the  $W_{ad}$  is, the stronger the bonding between interface atoms is. The  $W_{ad}$  of the interface can be given by [30,31]:

$$W_{ad} = \frac{1}{A} (E_{Ti} + E_{TiN} - E_{Ti/TiN}) \quad (16)$$

where  $E_{Ti}$  and  $E_{TiN}$  are the total energy of Ti slab and TiN slab after full relaxation, respectively;  $E_{Ti/TiN}$  is the total energy of the interface system; A is the interface area. The  $W_{ad}$  and interface separation ( $d_0$ ) values of Ti(0 0 0 1)/TiN (1 1 1) interfacial models are listed in Table 8, in which 1.520 in bracket refers to initial interface separation. It can be clearly seen that the stability of the interface model is sorted according to  $W_{ad}$  as follows: Ti-OT < Ti-SL < Ti-TL < N-OT < N-SL < N-TL. Among them, the  $W_{ad}$  of N-TL interface is the largest (7.97 J/m<sup>2</sup>) and its  $d_0$  is the smallest (1.181 Å), which indicates that the adhesive strength of the N-TL interface is the strongest among all of interfaces.

#### 3.4.3. Interface stability

The interfacial energy ( $\gamma$ ) is an important parameter to measure the stability of the interface. Generally, the smaller the  $\gamma$  is, the more stable the interface is. The  $\gamma$  can be given by [28,32]:

$$\gamma = \sigma_{Ti} + \sigma_{TiN} - W_{ad} \quad (17)$$

where  $\sigma_{\text{Ti}}$  and  $\sigma_{\text{TiN}}$  are the surface energy of Ti(0 0 0 1) and TiN(1 1 1) models;  $W_{ad}$  is the adhesive work of Ti/TiN interface.

The  $\gamma$  of Ti (0 0 0 1)/TiN (1 1 1) interface models are listed in Table 9. According to  $\gamma$ , the interfacial stability is sorted as follows: NTL > N-SL > N-TL > Ti-TL > Ti-SL > Ti-OT. It can be seen that the stability of the Ti/N interface is larger than that of the Ti/Ti interface, and the  $\gamma$  values of Ti/N interface are all lower than zero, which indicates it is thermodynamic stable. Among Ti/N interfaces, the  $\gamma$  of NTL interface is the smallest ( $-3.86 \text{ J/m}^2$ ), which indicates that N-TL interface is the most stable.

### 3.4.4. Electronic structure and bonding

The bonding of the interfacial atoms depends on the interface electronic structure and bonding character, which can be characterized by electron density and charge density difference. The electron density can be obtained by calculation and the charge density difference can be obtained by Eq. (18) [33,34]:

$$\Delta\rho = \rho_{\text{total}} - \rho_{\text{Ti}(0001)} - \rho_{\text{TiN}(111)} \quad (18)$$

where  $\rho_{\text{total}}$  is the total charge density of the Ti/TiN interface;  $\rho_{\text{Ti}(0001)}$  and  $\rho_{\text{TiN}(111)}$  are the charge densities of isolated Ti(0 0 0 1) slab and TiN (1 1 1) slab, respectively.

The charge density of the six Ti/TiN interfaces taken along the (2 1 1 0) direction ( $\text{e}/\text{\AA}^3$ ) is shown in Fig. 10. From Fig. 10(a)–(c), the chemical bonds are formed between interfacial atoms of Ti side and TiN side in all the Ti/N interface models, but the strength of bonding is different. In the three interface structures of the Ti/N, the electrons are obviously aggregated on the side of the N atom of TiN side, the bonding between the N atom of TiN side and the Ti atom of Ti is strong. From Fig. 10(b) and (c), in N-SL and N-TL interfaces, the first layer atoms of the Ti side is not only significantly bonded to the first layer atoms (N) of the TiN side, but also have weak bonding with the second layers atoms (Ti) of Ti side. Therefore, the bonding strengths and stabilities of N-SL interface and N-TL interface are larger than those of the N-OT interface, and the bonding strength of N-TL is slightly larger than that of T-SL. From Fig. 10(d)–(f), the bonding strength between the Ti atoms on the two sides of Ti/Ti interface is relatively weak, and the interface spacing is large, which suggests that the atoms on both sides of the Ti/Ti interface have only a weak bond. From the above analysis, the bonding strength of atoms at the interface of Ti/N interface model is larger than that of Ti/Ti interface model, so N-TL interface is most stable. The charge density difference of Ti/TiN interfaces taken along the (2 1 1 0) direction ( $\text{e}/\text{\AA}^3$ ) is shown in Fig. 11. From Fig. 11(a)–(c), the charges transfer from interfacial Ti atom of Ti side to the N atom of TiN side, and the charge is accumulated toward the N atom, which proves certain ionic feature besides covalent bonding. In N-SL and N-TL interfaces, the first layer atoms (Ti) on the Ti side also forms a weak bonding with the second layer atoms Ti of the TiN side, but its bond strength is significantly lower than that of the Ti-N covalent bond. It indicates that the Ti/N interface atoms form polar covalent bond and weak metal bond, in which the N-TL interface model has the strongest bond. From Fig. 11(d)–(f), the bonding strength of the Ti/Ti interfaces is obviously lower than that of the Ti/N interfaces. The charge aggregation between the Ti atom of Ti side and the Ti atom of TiN side at the Ti/Ti interfaces is weak, which indicates that the bonding between the Ti atom of Ti side and the Ti atom of TiN side at the interface is weak. From the above analysis, the bonding strength of Ti/N interface is obviously higher than that of Ti/Ti interface, which is in agreement with the above analysis of Fig. 10. Therefore, only the DOS of atoms Ti/ N interfaces is calculated, and the electronic structures of the interfaces are further clarified.

The DOS of Ti/N interfacial atoms is shown in Fig. 12. The DOS of the three interfacial atoms all are not zero at Fermi level, which indicates that the interfaces have certain metallic properties. It is obvious that the peaks at Fermi level are mainly composed of Ti-3d orbital in Ti interface side. Fig. 12(a) is the DOS of N-OT interfacial atoms. By analysis of PDOS, from  $-7.28$  eV and  $-1.79$  eV, the peak shape of the N-2p orbital is basically consistent with that of Ti-3d orbital, which indicates that the strong hybridization is formed between the N-2p and Ti-3d electrons. The DOS of Ti-3d orbital is slightly larger than that of N-2p orbital, which means that the contribution of Ti-3d orbital is slightly larger than that of N-2p orbital. Fig. 12(b) is the DOS of the NST interfacial atoms. By analysis of PDOS, within the scope of  $-7.52$  eV and  $-1.75$  eV, Ti-3d and N-2p electron orbitals resonate obviously and the contribution of Ti-3d orbital is much larger than that of N-2p orbital, which indicates that ionic bond and polar covalent bond are formed. From the Fig. 12(c), by analysis of total DOS, the DOS peak of N-TL interfacial atoms is the most sharp and its pseudogap is the widest in three Ti/N interfaces, which indicates that it is the strongest covalent bonding interaction. By analysis of PDOS, from  $-7.60$  eV to  $-2.55$  eV, the Ti-3d and N-2p orbitals have a strong interaction, which further indicates that strong covalent bond is formed in N-TL interface.

To further understand the interface charge transfer, the Bader charge is analyzed. Bader charges of bulk Ti and TiN, N-OT, N-SL and N-TL interfacial atoms are listed in Table 10. By comparing Bader charges between the bulk and interface, it is found that the interfacial Ti atoms at the interface of N-OT, N-SL and N-TL interfaces lose some charges (about 0.39–0.40, 0.80–0.81, and 0.81–0.82, respectively). Meanwhile, the interfacial N atoms of N-OT and N-SL interface loses some charges, which indicates that the amount of charge obtained of interfacial N atoms is decreased. However, the interfacial N atoms of the N-TL interface obtains some charges (about 0.088–0.094), which indicates that the charge amount of interfacial N atoms is increased. From the above analysis, the charge reduction of interfacial Ti atoms for the N-TL interface is larger than that of interfacial Ti atoms for N-OT and NSL interfaces and the charge acquisition of interfacial N atoms for the N-TL interface is larger than that of interfacial N atoms for N-OT and N-SL interfaces, which indicates that the bonding strength between the interfacial atoms of the N-TL interface is higher than that of the NOT and N-SL interfaces.

#### 4. Conclusion

(1) The lattice misfit between Ti (0 0 0 1)/TiN (1 1 1) interface is 2.46%, which indicates that Ti (0 0 0 1) and TiN (1 1 1) planes can make good lattice matching. (2) The bond of bulk Ti is strong metallicity, while that of bulk TiN is a mixture of covalent and metallic bonds. Six interfaces are built based on the lattice misfit and stacking modes. The interface bondings of the Ti/Ti interface models are all metal bond, and the bonding strength is relatively weak. The interfacial bonding strength of Ti/N interface is higher than that of the Ti/Ti interface, and interfacial bonding of Ti/N interface is a mixture of covalent, metallic and ionic bonds. (3) The binding strength between the interfaces can be described qualitatively by Wad. the larger the interface is, the more stable the interface model is. Among six interface models, the Wad of N-TL interface is the largest ( $7.97$  J/m<sup>2</sup>) and its d0 is smallest (1.181 Å), which indicates that the adhesive strength of the N-TL interface is the strongest among all of interfaces. (4) Generally, the smaller the  $\gamma$  is, the more stable the interface is. According to  $\gamma$ , the interfacial stability is sorted as follows: NTL > N-SL > N-TL > Ti-TL > Ti-SL > Ti-OT. It can be seen that the stability of the Ti/N interface is larger than that of the Ti/Ti interface, and the  $\gamma$  of Ti/N interface are all lower than zero, which indicates that it is thermodynamic stable. Among Ti/N interfaces,

the  $\gamma$  of N-TL interface is the smallest ( $-3.86 \text{ J/m}^2$ ), which indicates that N-TL interface is the most stable.

## 5. CRediT authorship contribution statement

The manuscript was written through contributions of all authors. All authors have given approval to the final version of the manuscript. Qingxiang Yang contributed to the conception of the study; Lixiang Rao performed the data analyses and wrote the manuscript; Sha Liu and Zhijun Shi provided the guidance of calculation; Huan Liu contributed significantly to analysis and manuscript preparation; Yefei Zhou and Xuejun Ren performed the analysis with constructive discussions.

## Acknowledgement

The authors would like to express their gratitude for projects supported by the National Natural Science Foundation of China (No. 51471148 and No. 51771167), the Hebei province Basic Research Foundation of China (No. 16961008D).

## References

- [1] G. Ryan, A. Pandit, D.P. Apatsidis, Fabrication methods of porous metals for use in orthopaedic applications, *Biomaterials* 27 (2006) 2651–2670.
- [2] C. Leyens, M. Peters, *Titanium and Titanium Alloys: Fundamentals and Applications*, Wiley-VCH, Germany, 2003, pp. 181–188.
- [3] E. Brandl, F. Palm, V. Michailov, B. Viehweger, C. Leyens, Mechanical properties of additive manufactured titanium (Ti-6Al-4V) blocks deposited by a solid-state laser and wire, *Mater. Des.* 32 (2011) 4665–4675.
- [4] V. Koshuro, A. Fomin, I. Rodionov, Composition, structure and mechanical properties of metal oxide coatings produced on titanium using plasma spraying and modified by micro-arc oxidation, *Ceram. Int.* 44 (2018) 12593–12599.
- [5] Y.H. Diao, K.M. Zhang, Microstructure and corrosion resistance of TC2 Ti alloy by laser cladding with Ti/TiC/TiB<sub>2</sub> powders, *Appl. Surf. Sci.* 352 (2015) 163–168.
- [6] E. Marin, R. Offoia, M. Regis, S. Fusi, A. Lanzutti, L. Fedrizzi, Diffusive thermal treatments combined with PVD coating for tribological protection of titanium alloys, *Mater. Des.* 89 (2016) 314–322.
- [7] W.G. Kim, H.C. Choe, Effects of TiN coating on the corrosion of nanostructured Ti-30Ta-xZr alloys for dental implants, *Appl. Surf. Sci.* 258 (2012) 1929–1934.
- [8] N.M. Lin, X.B. Huang, X.G. Zhang, A.L. Fan, L. Qin, B. Tang, In vitro assessments on bacterial adhesion and corrosion performance of TiN coating on Ti6Al4V titanium alloy synthesized by multi-arc ion plating, *Appl. Surf. Sci.* 258 (2012) 7047–7051.
- [9] W. Feng, D.R. Yan, J.N. He, X.Z. Li, Y.C. Dong, Reactive plasma sprayed TiN coating and its tribological properties, *Wear* 258 (2005) 806–811.
- [10] M.W. Finnis, The theory of metal-ceramic interfaces, *J. Phys.: Condens. Matter* 8 (1996) 5811–5843.
- [11] M.W. Finnis, C. Kruse, U. Schönberger, Ab Initio calculations of metal/ceramic interfaces: what have we learned, what can we learn? *Nanostruct. Mater.* 6 (1995) 145–155.
- [12] H.H. Xiong, H.N. Zhang, J.H. Dong, Adhesion strength and stability of TiB<sub>2</sub>/TiC interface in composite coatings by first principles calculation, *Comput. Mater. Sci.* 127 (2017) 244–250.
- [13] X.W. Fan, B. Chen, M.M. Zhang, D. Li, Z. Liu, C.Y. Xiao, First-principles calculations on bonding characteristic and electronic property of TiC(111)/TiN (111) interface, *Mater. Des.* 112 (2016) 282–289.
- [14] C.Y. Liu, N. Jin, Z.Q. Li, X.D. Liu, First-principles calculations on the electronic

- structure and bonding nature of TaN(111)/TiN(111) interface, *J. Alloy. Compd.* 717 (2017) 326–332.
- [15] G. Kresse, J. Furthmüller, Efficient iterative schemes for ab initio total-energy calculations using a plane-wave basis set, *Phys. Rev. B* 54 (1996) 11169–11186.
- [16] G. Kresse, D. Joubert, From ultrasoft pseudopotentials to the projector augmentedwave method, *Phys. Rev. B* 59 (1999) 1758–1775.
- [17] P.E. Blochl, Projector augmented-wave method, *Phys. Rev. B* 50 (1994) 17953–17979.
- [18] H.J. Monkhorst, J.D. Pack, Special points for Brillouin-zone integrations, *Phys. Rev. B* 13 (1976) 5188–5192.
- [19] J. Yang, X. Hou, P. Zhang, Y. Zhou, X. Xing, X. Ren, et al., First-principles calculations on LaAlO<sub>3</sub> as the heterogeneous nucleus of austenite, *Comput. Theor. Chem.* 1029 (2014) 48–56.
- [20] S. Cardinal, A. Malchère, V. Garnier, G. Fantozzi, Microstructure and mechanical properties of TiC-TiN based cermets for tools application, *Int. J. Refract. Met. Hard. Mater.* 27 (2009) 521–527.
- [21] C. Stampfl, W. Mannstadt, R. Asahi, A.J. Freeman, Electronic structure and physical properties of early transition metal mononitrides: density-functional theory LDA, GGA, and screened-exchange LDA FLAPW calculations, *Phys. Rev. B* 63 (2001) 155106.
- [22] D. Gall, S. Kodambaka, M.A. Wall, I. Petrov, J.E. Greene, Pathways of atomistic processes on TiN (001) and (111) surfaces during film growth: an ab initio study, *J. Appl. Phys.* 93 (2003) 9086–9094.
- [23] R.R. Pawar, V.T. Deshpande, The anisotropy of the thermal expansion of  $\alpha$ -titanium, *Acta Cryst. A* 24 (1968) 316.
- [24] Y.F. Li, Y.M. Gao, B. Xiao, T. Min, Y. Yang, S.Q. Ma, D.W. Yi, The electronic, mechanical properties and theoretical hardness of chromium carbides by first-principles calculations, *J. Alloy. Compd.* 509 (2011) 5242–5249.
- [25] R. Gaillac, P. Pullumbi, F.X. Coudert, ELATE: an open-source online application for analysis and visualization of elastic tensors, *J. Phys.: Condens. Matter* 28 (2016) 275201 (5 pp).
- [26] W. Setyawan, S. Curtarolo, High-throughput electronic band structure calculations: challenges and tools, *Comput. Mater. Sci.* 49 (2010) 299–312.
- [27] B.L. Bramfitt, The effect of carbide and nitride additions on the heterogeneous nucleation behavior of liquid iron, *Metall. Mater. Trans. B* 1 (1970) 1987–1990.
- [28] J. Boettger, Nonconvergence of surface energies obtained from thin-film calculations, *Phys. Rev. B* 49 (1994) 16798–16800.
- [29] L.M. Liu, S.Q. Wang, H.Q. Ye, First-principles study of polar Al/TiN(111) interfaces, *Acta. Mater.* 52 (2004) 3681–3688.
- [30] S.Q. Wang, H.Q. Ye, Theoretical studies of solid-solid interfaces, *Curr. Opin. Solid State Mater. Sci.* 10 (2006) 26–32.
- [31] W.Y. Choe, G.J. Miller, E.M. Levin, Crystal structure and magnetism of Gd<sub>2</sub>MgGe<sub>2</sub>, *J. Alloy. Compd.* 329 (2001) 121–130.
- [32] Y.J. Xian, R.Z. Qiu, X. Wang, P.C. Zhang, Interfacial properties and electron structure of Al/B<sub>4</sub>C interface: a first-principles study, *J. Nucl. Mater.* 478 (2016) 227–235.
- [33] J. Boettger, Nonconvergence of surface energies obtained from thin-film calculations, *Phys. Rev. B* 49 (1994) 16798–16800.
- [34] V. Fiorentini, M. Methfessel, Extracting convergent surface energies from slab calculations, *J. Phys. Condens. Matter* 8 (1996) 6525–6529.

**Table 8**  
Relaxed  $d_0$  and  $W_{ad}$  for the Ti(0 0 0 1)/TiN(1 1 1) interface models.

Termination	Stacking	Relaxed	
		$d_0$ (Å)	$W_{ad}$ (J/m <sup>2</sup> )
Ti/N	OT	1.875(1.520)	4.86
	SL	1.316(1.520)	7.06
	TL	1.181(1.520)	7.97
Ti/Ti	OT	2.619(1.520)	2.56
	SL	2.413(1.520)	2.95
	TL	2.372(1.520)	3.13

**Table 1**  
Calculated results of relaxed TiN bulk compared with other published papers.

System	Method	Lattice constants $a$ (Å)	Bulk modulus $K$ (GPa)	Formation energy $E_{for}$ (GPa)
TiN		4.24	308.39	-3.50
	GGA-PBE <sup>a</sup>	4.25	266	-3.94
	GGA-PW91 <sup>b</sup>	4.245	279.15	-
	LDA-FLAPW <sup>c</sup>	4.18	329	-4.36
	Expt	4.24 <sup>d</sup>	320 <sup>e</sup>	-3.50 <sup>e</sup>

<sup>a</sup> Ref. [13]. <sup>b</sup> Ref. [14]. <sup>c</sup> Ref. [20]. <sup>d</sup> Ref. [21]. <sup>e</sup> Ref. [22].

**Table 2**  
Elastic properties of bulk TiN.

Averaging scheme	Bulk modulus	Young's modulus	Shear modulus	Poisson's ratio
Voigt	308.39 GPa	496.13 GPa	201.37 GPa	0.23187
Reuss	308.39 GPa	473.86 GPa	190.47 GPa	0.2439
Hill	308.39 GPa	485.05 GPa	195.92 GPa	0.23786

**Table 3**  
Variations of the elastic moduli for bulk TiN.

	Young's modulus		Linear compressibility		Shear modulus		Poisson's ratio	
	$E_{min}$	$E_{max}$	$\beta_{min}$	$\beta_{max}$	$G_{min}$	$G_{max}$	$\nu_{min}$	$\nu_{max}$
Value	411.98 GPa	611.68 GPa	1.0809 TPa <sup>-1</sup>	1.0809 TPa <sup>-1</sup>	161.26 GPa	261.53 GPa	0.12425	0.39087
Anisotropy	1.485		1		1.622		3.1459	
Axis	0.5774	0.0000	0.0000	0.5000	0.0000	0.7071	0.7071	0.7071
	0.5774	0.0000	0.0000	0.0000	0.0000	-0.0003	0.0000	0.0000
	0.5773	1.0000	1.000	0.8660	1.0000	0.7071	0.7071	-0.7071
Second axis					1.0000	0.7071	0.0000	-0.7071
					0.0002	-0.0005	1.0000	0.0002
					0.0000	-0.7071	0.0000	-0.7071

**Table 4**  
Planar lattice misfit between Ti and TiN interface.

Matching interface	Ti(0 0 0 1)//TiN(1 1 1)			Ti(0 0 0 1)//TiN(1 0 0)			Ti(1 1 2 0)//TiN(1 0 0)	
[u v w]Ti	[2 1 1 0]	[1 1 0 0]	[1 2 1 0]	[2 1 1 0]	[1 1 0 0]	[1 2 1 0]	[1 1 0 0]	[0 0 0 1]
[u v w]TiN	[1 0 1]	[2 1 1]	[1 1 0]	[0 1 0]	[1 1 0]	[1 0 0]	[0 1 0]	[1 0 0]
$\theta(^{\circ})$	0	0	0	15	0	15	0	2.556
$d_{\text{Ti}}$ (Å)	2.923	5.063	2.923	2.923	5.063	2.923	5.063	4.631
$d_{\text{TiN}}$ (Å)	2.997	5.190	2.997	2.119	2.997	2.119	4.238	4.238
$\delta$ (%)	2.46			14.41			22	

**Table 5**  
Calculated surface energy of Ti(0 0 0 1) surface models.

Layer (N)	5	6	7	8	9
Surface energy (J/m <sup>2</sup> )	2.00	1.92	1.95	1.96	1.96

**Table 6**  
Calculated surface energy of TiN(1 1 1) Ti-terminated surface models.

Layer (N)	3	5	7	9	11
Surface energy (J/m <sup>2</sup> )	7.11	5.76	4.68	4.67	4.66

**Table 7**  
Calculated surface energy of TiN(1 1 1) N-terminated surface models.

Layer (N)	5	7	9	11	13	15
Surface energy (J/m <sup>2</sup> )	2.24	2.13	2.24	2.16	2.18	2.15

**Table 9**  
Interface energy of the Ti(0 0 0 1)/TiN(1 1 1) interfaces.

Model	N-OT	N-SL	N-TL	Ti-OT	Ti-SL	Ti-TL
$\gamma$ (J/m <sup>2</sup> )	-0.75	-2.95	-3.86	4.08	3.68	3.51

**Table 10**  
Bader charges of bulk Ti and TiN, NOT, NSL and NTL interfacial atoms.

Systems	Charges of Ti	Charges of N
Bulk Ti	3.9952–4.0048	
Bulk TiN	2.4908	6.5060–6.5123
N-OT interface	3.6097	6.3185
N-SL interface	3.1940	6.4678
N-TL interface	3.1859	6.6003

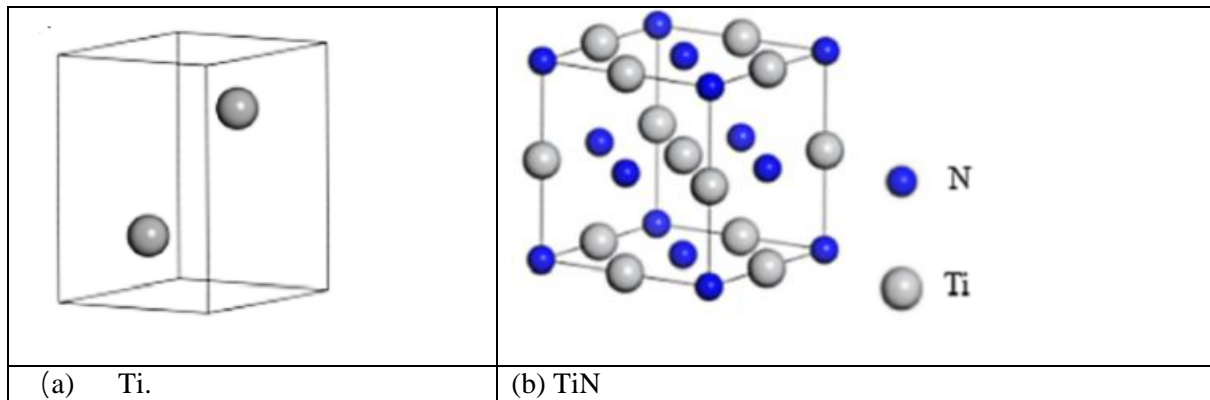


Figure 1 Relaxed crystal structures of (a) Ti and (b) TiN.

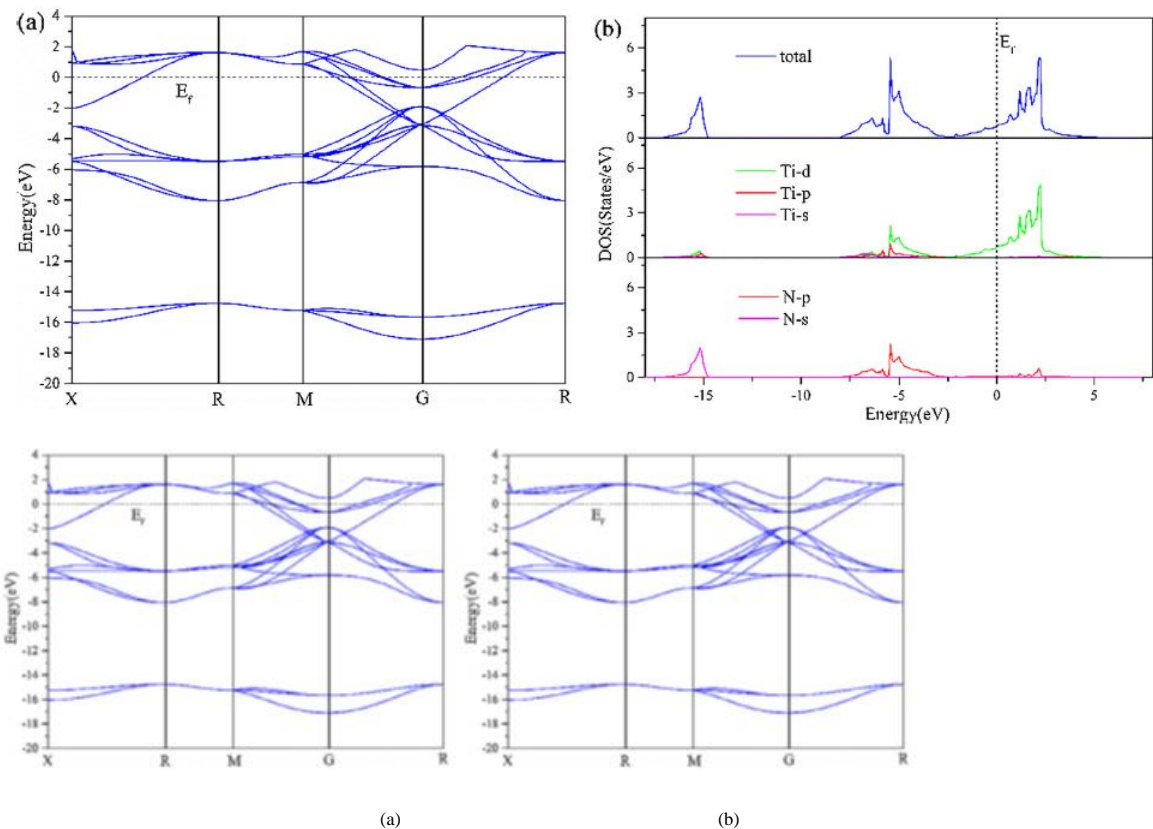


Figure 2. Calculated band structure (a) and density of states (b) of TiN. The Fermi level is indicated by dashed line.

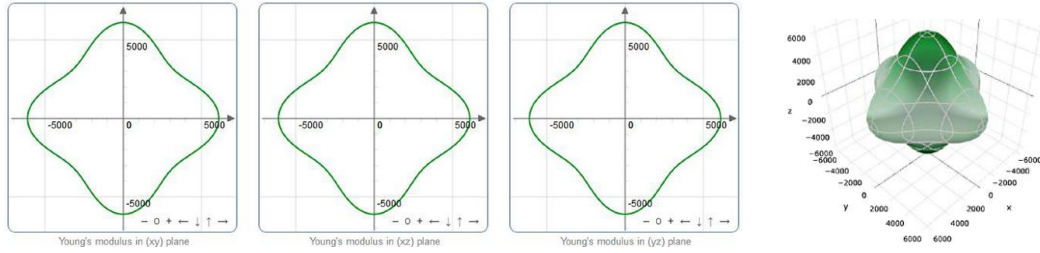


Figure. 3. Spatial dependence of Young's modulus.

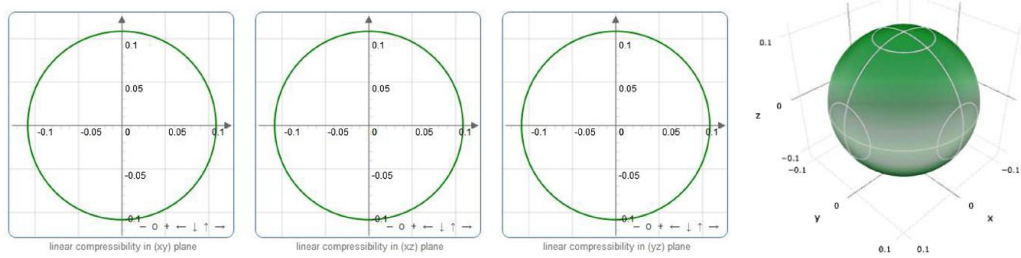


Figure. 4. Spatial dependence of Linear compressibility.

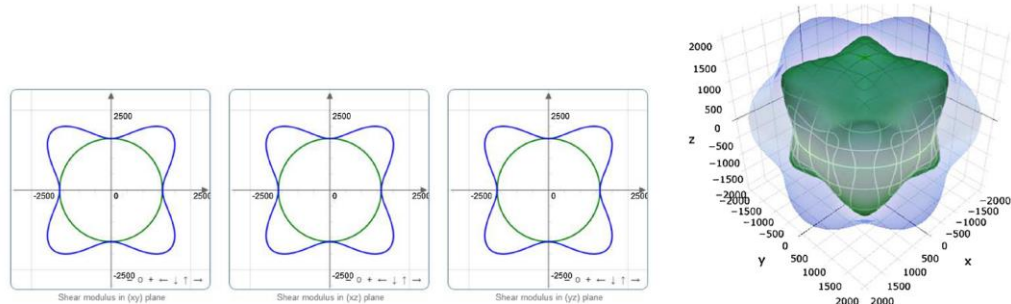


Figure. 5. Spatial dependence of Shear modulus

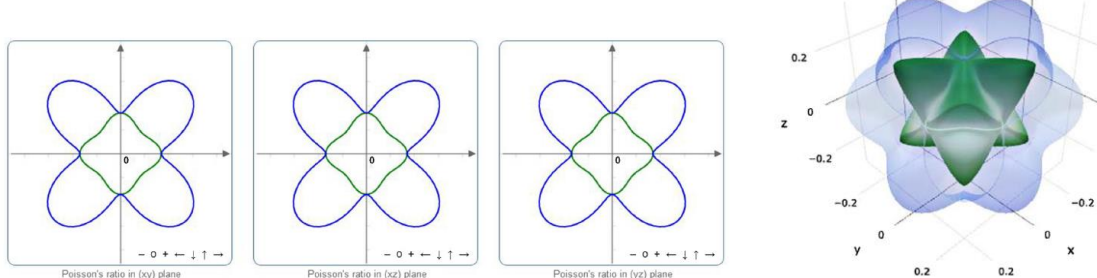
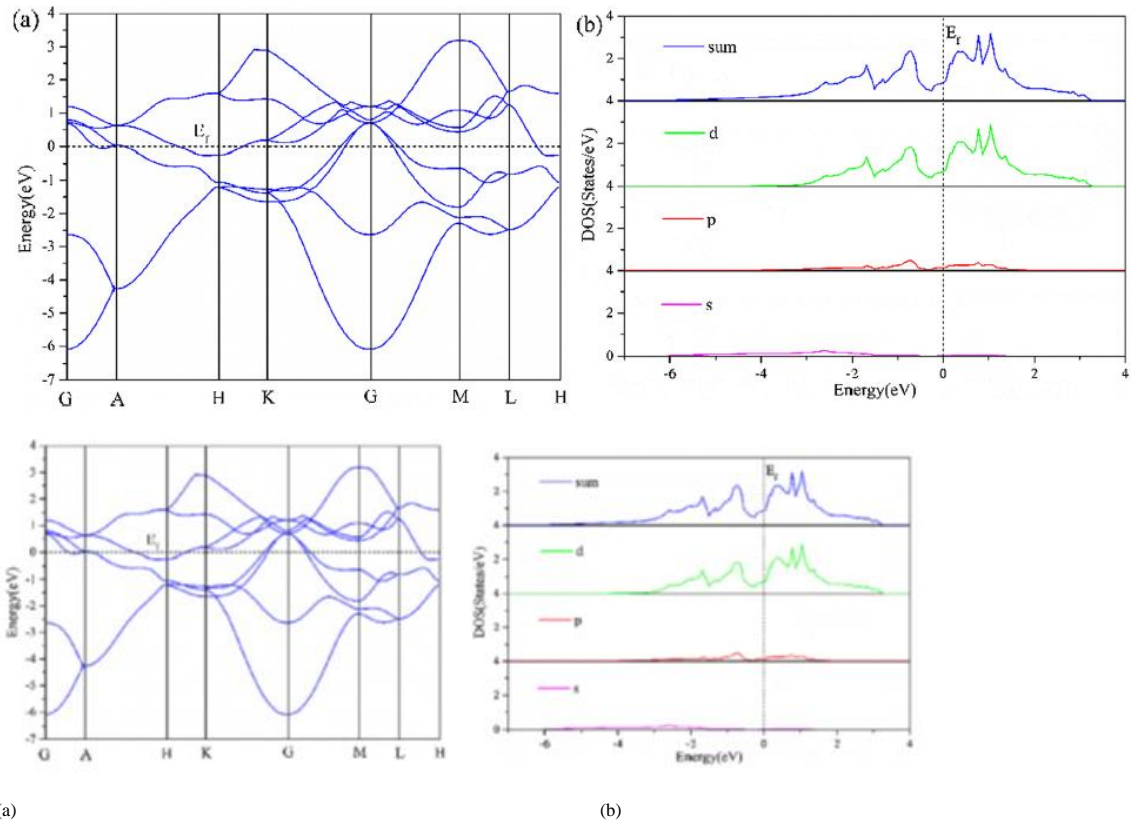


Figure 6. Spatial dependence of Poisson's ratio.



(a)

(b)

Figure 7 Calculated band structure (a) and density of states (b) of Ti. The Fermi level is indicated by dashed line.

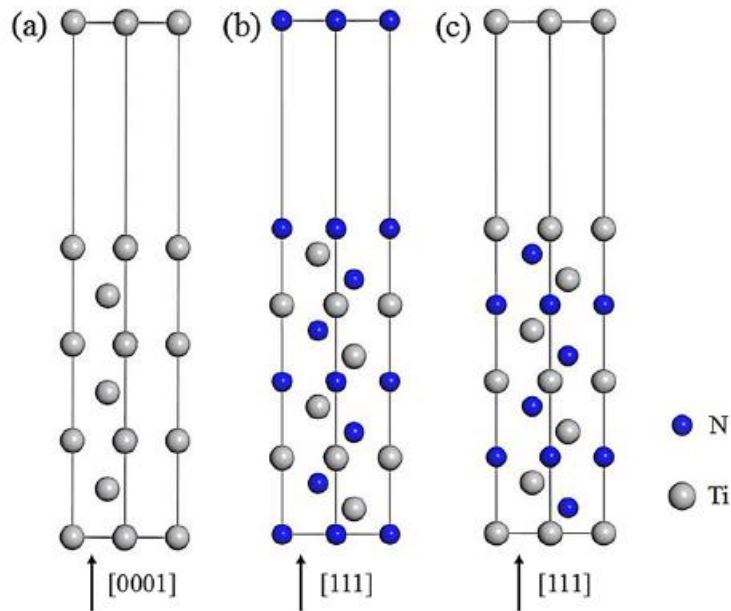


Figure 8. Surface models of Ti and TiN. (a)  $\text{Ti}(0\ 0\ 0\ 1)$ , (b)  $\text{TiN}(1\ 1\ 1)$  Ti-terminated, c)  $\text{TiN}(1\ 1\ 1)$  N-terminated.

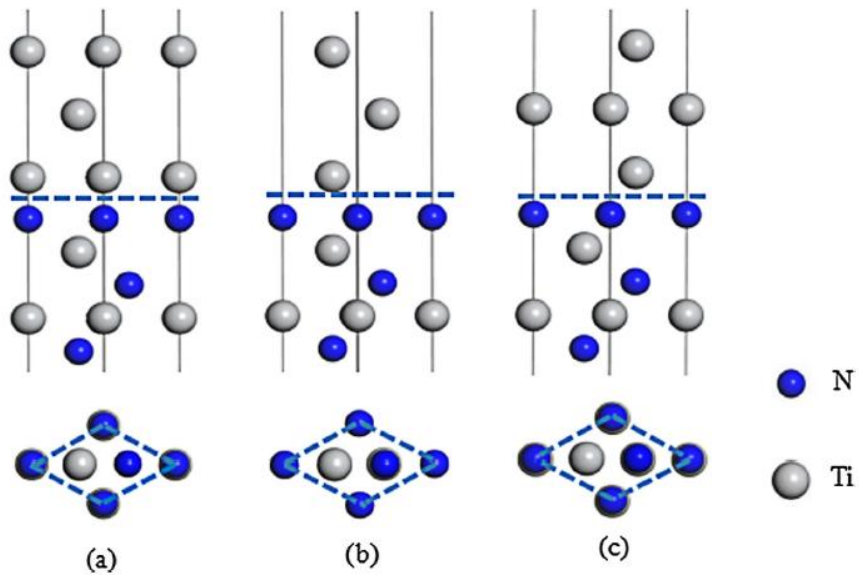


Figure 9 Schematic plots of (a) OT, (b) (SL), (c) TL stacking sequences.

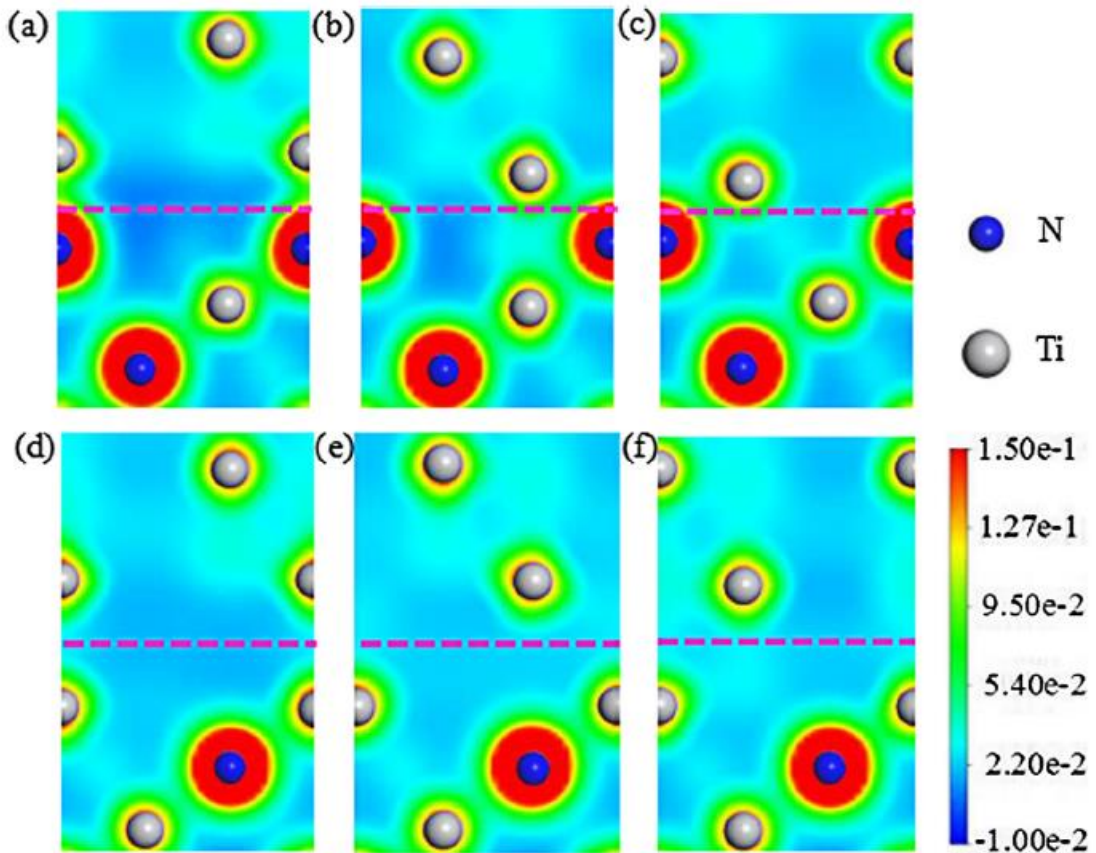


Figure 10. Charge density of Ti/TiN interfaces taken along the (2 1 1 0) direction ( $e/\text{\AA}^3$ ). (a) N-OT interface, (b) N-SL interface, (c) N-TL interface, (d) Ti-OT interface, (e) Ti-SL interface.

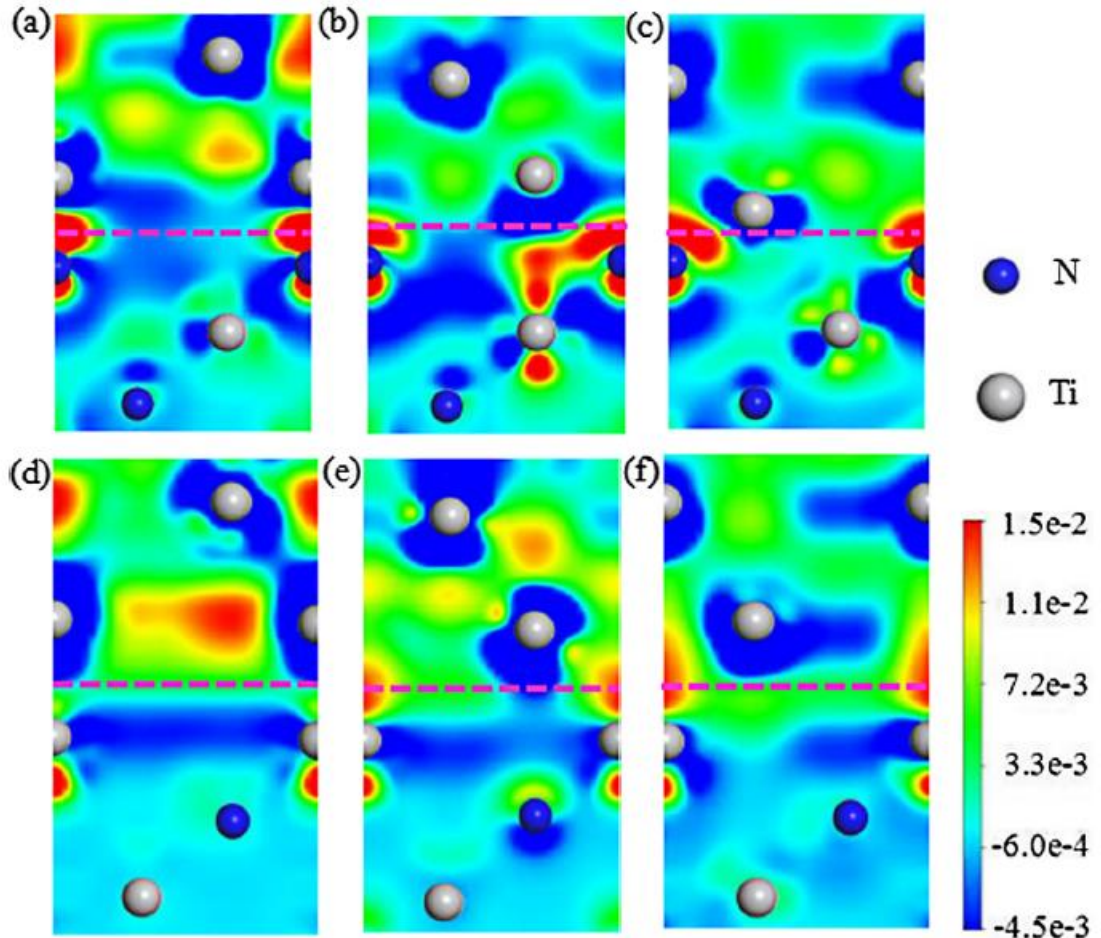


Figure Charge density difference of Ti/TiN interfaces taken along the  $(2\bar{1}10)$  direction ( $e/\text{\AA}^3$ ). (a) N-OT interface, (b) N-SL interface, (c) N-TL interface, (d) Ti-OT interface, (e) Ti-SL interface, (f) Ti-TL interface. The horizontal dashed lines indicate the location of the interfaces.

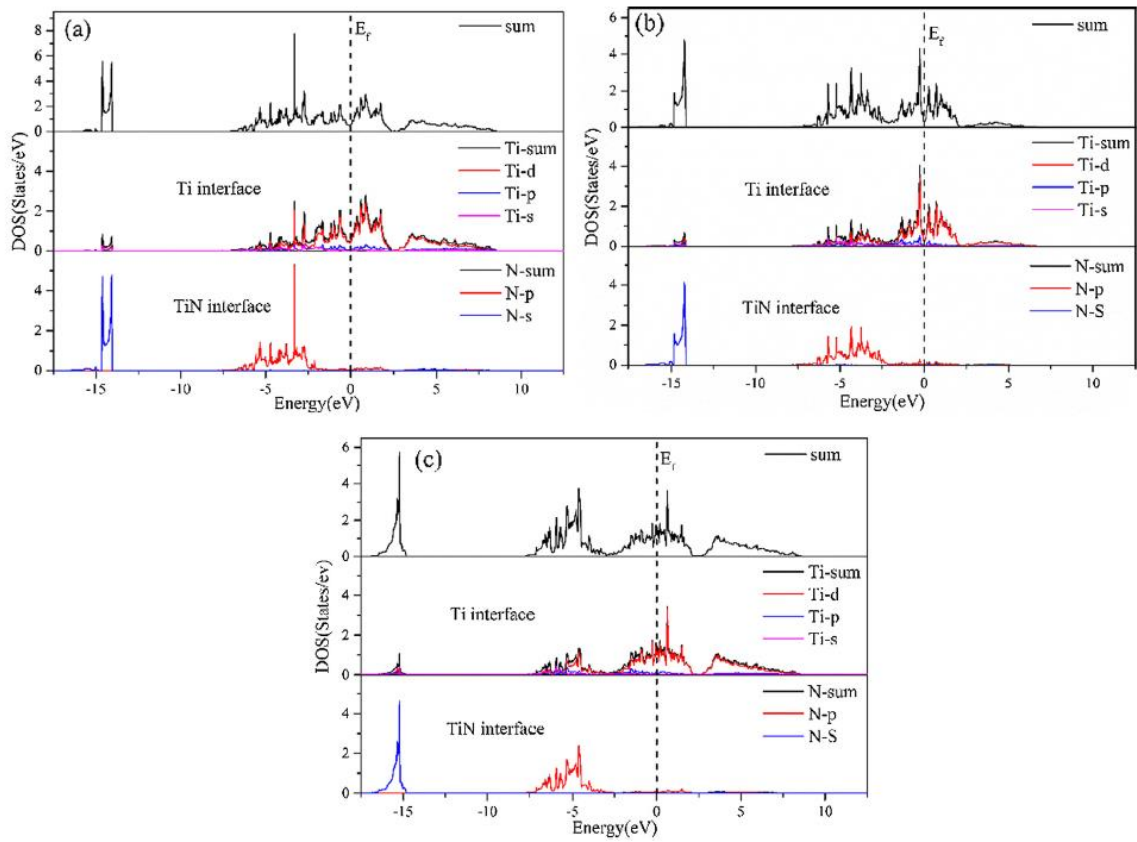


Figure 12. DOS for (a) N-OT interfacial atoms, (b) N-SL interfacial atoms, (c) N-TL interfacial atoms, respectively.